

Optimal location of a new interferometric gravitational wave observatoryAntony C. Searle,^{*} Susan M. Scott,[†] and David E. McClelland[‡]*Centre for Gravitational Physics, Department of Physics, Faculty of Science, The Australian National University, Canberra ACT 0200 Australia*

L. Samuel Finn

Center for Gravitational Wave Physics, Department of Physics, Astronomy and Astrophysics, The Pennsylvania State University, 104 Davey Laboratory, PMB#145, University Park, Pennsylvania 16802, USA

(Received 8 November 2005; revised manuscript received 24 April 2006; published 12 June 2006)

As gravitational wave astronomy becomes a reality, issues of how to best combine and expand the global network of observatories will come to the fore. We have constructed several models to determine optimal additions to an existing global network of observatories for certain gravitational wave source populations and detection strategies.

DOI: [10.1103/PhysRevD.73.124014](https://doi.org/10.1103/PhysRevD.73.124014)

PACS numbers: 04.30.Db, 95.55.Ym

I. INTRODUCTION

When multiple gravitational wave observatories are analyzed as a single instrument, in a process analogous to aperture synthesis in radio astronomy, the relative locations of the observatories become important. The baselines between the detectors are also important for triangulation of gravitational wave sources. The relative orientations of the antenna patterns of observatories affects their ability to detect any particular signal. As both the baselines and antenna patterns are dictated by the siting, these properties cannot be decoupled and independently optimized.

The detectability of a population of gravitational wave sources depends not only on these geometric factors, but also on the data analysis strategy employed. A single detector may be considered in an analysis, or data from multiple detectors may be analyzed cooperatively. If data from multiple detectors is to be considered, the data may be combined *coherently*, *incoherently* or in some intermediate way (as in a hierarchical search). An analysis may be limited by practical considerations of computational power or bandwidth. Fully coherent searches over large signal parameter spaces are typically computationally unfeasible. The sensitivity of realistic searches will typically lie between the coherent and incoherent cases.

A great deal of effort has gone into optimizing the performance of these analyses [1–6], but less work has been done on optimizing another component in the sensitivity: the siting of the component detectors. Ideally, future gravitational wave observatories should be located so as to optimize their contribution to the global network of gravitational wave detectors.

We expand upon initial results previously reported in [7], presenting models of the relative collective sensitivity of a global collaboration of gravitational wave detectors, to

determine the relative sensitivities of future configurations to a variety of possible sources, and to develop recommendations as to the configuration and expansion of the network.

In this paper we determine the optimal location for new observatories to supplement various existing networks, for the case of a uniform population of binary inspiral events detected by either coincident or coherent analysis, and for the case of a galactic population of continuous wave sources.

II. METHODOLOGY

Consider a reference frame corotating with the Earth. Define twin Cartesian $[x, y, z]$ and spherical polar $[r, \theta, \phi]$ coordinate systems with their origins at the center of the Earth (assumed to be a perfect sphere) such that

$$[x, y, z] = [r \cos\theta \cos\phi, r \cos\theta \sin\phi, r \sin\theta], \quad (1)$$

where θ and ϕ correspond to latitude North and longitude East, respectively, (in radians). Along any line of constant θ and ϕ , the orthonormal unit vectors *local North* $\hat{\theta}$ and *local East* $\hat{\phi}$ may be defined in Cartesian coordinates:

$$\begin{aligned} \hat{\theta} &= [-\sin\theta \cos\phi, -\sin\theta \sin\phi, \cos\theta], \\ \hat{\phi} &= [-\sin\phi, \cos\phi, 0]. \end{aligned} \quad (2)$$

A horizontal interferometric gravitational wave observatory at sea level with mutually perpendicular arms of equal length may be described by its latitude θ , longitude ϕ and the *orientation* angle ψ (in radians) of its x -arm clockwise from local North. The unit vectors along the arms are

$$\hat{\mathbf{e}}_x = \hat{\theta} \cos\psi + \hat{\phi} \sin\psi, \quad \hat{\mathbf{e}}_y = \hat{\theta} \sin\psi - \hat{\phi} \cos\psi. \quad (3)$$

The response m of an ideal such detector [2] to incident strain \mathbf{H} is purely geometric and given by

^{*}Electronic address: antony.searle@anu.edu.au

[†]Electronic address: susan.scott@anu.edu.au

[‡]Electronic address: david.mcclelland@anu.edu.au

$$m = \sum_{i,j=1}^3 R_{ij} H_{ij}, \quad (4)$$

where

$$\mathbf{R} = \frac{1}{2}(\hat{\mathbf{e}}_x^T \hat{\mathbf{e}}_x - \hat{\mathbf{e}}_y^T \hat{\mathbf{e}}_y). \quad (5)$$

Similarly to an interferometer, a source of gravitational radiation can be instantaneously described [2] in terms of the latitude θ and longitude ϕ for which it is overhead (i.e., it lies on the line of sight θ , ϕ) and an orientation angle ψ (required to uniquely determine the polarizations) from North $\hat{\theta}$. The x and y axes of the source are then as in Eq. (3), producing a *polarization basis*

$$\hat{\mathbf{E}}_+ = \hat{\mathbf{e}}_x^T \hat{\mathbf{e}}_x - \hat{\mathbf{e}}_y^T \hat{\mathbf{e}}_y, \quad \hat{\mathbf{E}}_\times = \hat{\mathbf{e}}_x^T \hat{\mathbf{e}}_y + \hat{\mathbf{e}}_y^T \hat{\mathbf{e}}_x. \quad (6)$$

The time-dependent strain $\mathbf{H}(t)$ produced by plane gravitational waves may then be described in this basis by the two functions of time h_+ and h_\times , so that

$$\mathbf{H}(t) = h_+(t) \hat{\mathbf{E}}_+ + h_\times(t) \hat{\mathbf{E}}_\times \quad (7)$$

in the limit where $t \ll T_{\text{sidereal}}$, i.e., when the rotation of the Earth does not significantly change the relative orientations of the source and detector over the duration of the signal; this is the case for binary inspiral events but not for continuous wave sources.

The *antenna patterns* [2]

$$F_+ = \sum_{i,j=1}^3 R_{ij} (\hat{\mathbf{E}}_+)_{ij}, \quad (8)$$

$$F_\times = \sum_{i,j=1}^3 R_{ij} (\hat{\mathbf{E}}_\times)_{ij}, \quad (9)$$

are a particular detector's response to the '+' or '×' polarizations. The detector's response to a signal described in that basis by $h_+(t)$ and $h_\times(t)$ is thus given by

$$m(t) = F_+ h_+(t) + F_\times h_\times(t). \quad (10)$$

The quantity

$$F_+^2 + F_\times^2 \quad (11)$$

is independent of the choice of polarization basis; it corresponds to the relative power received, from an unpolarized source in a particular direction, by an ideal detector.

Peak sensitivity occurs when the source is perpendicular to the plane of the arms; for a terrestrial detector, this corresponds to a source directly above or below. The detector is insensitive along the ‘‘arm diagonal’’ directions $\pm \hat{\mathbf{e}}_x \pm \hat{\mathbf{e}}_y$, where symmetry dictates that the strain on each arm is equal.

The geometrical properties of existing interferometric gravitational wave detectors have been collated in [8–10]. The antenna patterns of the different detectors may be compared in Fig. 1.

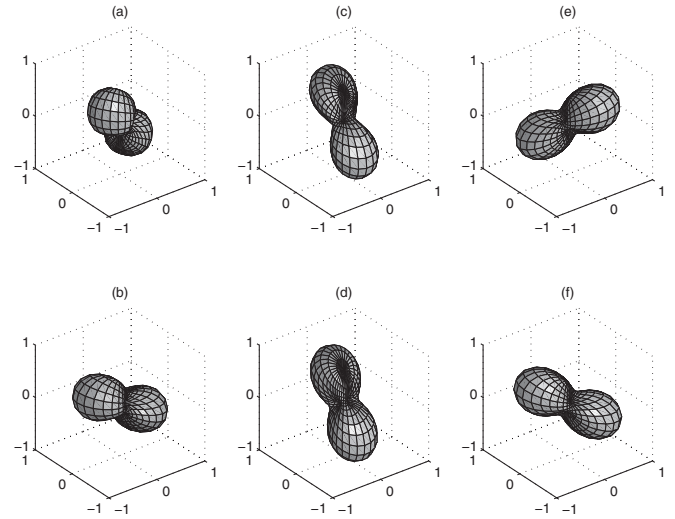


FIG. 1. Relative orientations of the antenna patterns of existing detectors (a) LIGO Hanford (both instruments), (b) LIGO Livingston, (c) VIRGO, (d) GEO, (e) TAMA and (f) proposed detector AIGO.

We will call a system of interferometric gravitational wave observatories and their cooperative data analysis technique a *network*, and present a simple formalism providing a general basis for the comparison of networks under certain criteria. Computationally-amenable *figures of merit* approximating significant properties of the network—such as the rate of detections produced by the set of observatories for a given gravitational wave source population under a given cooperative data analysis technique—are used to rank the relative performance of different networks.

Consider the set \mathcal{N} of all networks. A *figure of merit* f is defined as a real function on some subset \mathcal{S} of networks, $f: \mathcal{S} \subseteq \mathcal{N} \rightarrow \mathbb{R}$, for which $f(\alpha) > f(\beta)$ (where $\alpha \in \mathcal{S}$ and $\beta \in \mathcal{S}$) is interpreted as the statement that network α is better than network β . An example figure of merit that is mathematically straightforward (but of great practical importance) is the inverse of the cost of the construction of a network. There are many possible figures of merit and, in general, they will not produce the same rankings; assessment of the significance of the results of different figures of merit must be done by assessing the significance of the figures of merit themselves.

Figures of merit must be computationally tractable as well as significant. The restriction of the domain of the figure of merit to a particular subset $\mathcal{S} \subseteq \mathcal{N}$ of networks may simplify computation of the figure of merit while still permitting the examination of problems of interest. Frequently, this involves finding the optimal network or networks $\hat{\alpha}$ in a set $\mathcal{T} \subseteq \mathcal{S}$ which is determined by the constraints on the problem,

$$\hat{\alpha} = \{\beta: \beta \in \mathcal{T}, f(\beta) = \max_{\mathcal{T}} f\}. \quad (12)$$

Here we restrict ourselves to considering subsets $\mathcal{S} \subseteq \mathcal{N}$ of networks of fixed numbers of interferometric gravitational wave detectors, where all detectors in all networks in \mathcal{S} are assumed to be of identical design. A subset \mathcal{S} is completely described by the number n of detectors in a network, the “design” Θ of the identical detectors (arm length, sensitivity, noise floor ...) and the cooperative analysis method Ξ used. Any particular network $\alpha \in \mathcal{S}$ is then completely described by, for each detector, the latitudes θ_i and longitudes ϕ_i of the beam-splitters, and the orientation angles ψ_i of the x-arms clockwise from North (under the assumption of horizontal detectors on a perfectly spherical Earth). Each network is then a point in the $3n$ -dimensional parameter space $[(\theta_1, \phi_1, \psi_1), \dots, (\theta_n, \phi_n, \psi_n)]$.

We will consider *families* of figures of merit $f_{(n,\Theta,\Xi)}$; these permit comparisons of different geographical configurations of networks in a subset \mathcal{S} , but *not* comparisons of networks with different numbers of detectors n , designs Θ or analysis algorithms Ξ .

III. DETECTION OF BINARY INSPIRAL EVENTS

The theoretically-known waveforms of the inspiral phase of merging compact binary stellar systems is one of the most promising sources of gravitational waves for first-generation terrestrial interferometric observatories. For these observatories the events are rare, brief, and predominantly faint. The ability to distinguish between real signals and instrumental artifacts is the limiting factor. Combining data from multiple observatories can improve both sensitivity and confidence, by weeding out such artifacts. In fact, the twin LIGO observatories at Hanford and Livingston are intended to provide independent verification of each other’s results. Network analysis is the generalization of this concept.

The coincident network analysis technique [1,3], in its simplest form, allows independent searches to be performed by each detector in the network; a signal is only detected by the network when the signal is detected by each member detector. A more sophisticated technique is *coherent* network analysis [4,5], whereby the output of all detectors is collected and then a single search is performed on the combined data.

The twin LIGO sites were chosen to facilitate a coincidence analysis—they are distant enough to reduce common environmental disturbances and produce a measurable arrival time difference, but close enough to have similar antenna patterns [2] and so produce similar responses to an incident gravitational wave. Likewise, the location of the proposed Australian International Gravitational Observatory (AIGO) [11] has been selected to be near-antipodal to the LIGO sites thereby sharing their antenna patterns, while introducing a significant arrival time delay [12]. The sites of VIRGO, and the proposed Laser Cryogenic Gravitational Telescope (LCGT), however,

were not selected [13,14] to facilitate a global network analysis (nor could they be, given the locations of their originating countries). This implies that any realistic global network will likely be, in this sense, suboptimal and we will determine how significantly this will impact the ability of the network to do science with respect to a particular gravitational wave source population.

We define a figure of merit corresponding to the detection rate for a population of standard-candle binary inspiral events. Consider a particular class of binary inspiral systems, producing a particular deterministic gravitational waveform. Distribute these systems uniformly in flat space and randomly orient them. Let the distribution be unchanging in time so that any volume of space produces a constant rate of events. The property on which we will base the figure of merit $f_{(n,\Theta,\Xi)}$ is the rate at which inspiral events from this population may be confidently detected by the application of some network analysis algorithm Ξ to any given network of n gravitational wave detectors of design Θ .

A. Waveform and response

A simple binary inspiral [2] produces a quadrupole strain of the form

$$\mathbf{H} = \frac{\eta(t)}{r} (\hat{\mathbf{E}}_+ h_+(t) + \hat{\mathbf{E}}_\times h_\times(t)), \quad (13)$$

where

$$h_+(t) = (1 + \cos^2 \iota) \cos \zeta(t), \quad (14)$$

$$h_\times(t) = 2 \cos \iota \sin \zeta(t). \quad (15)$$

The parameter r is the distance traversed by the gravitational radiation, ι is the inclination angle of the source to the line of sight, and η and ζ depend on other properties of the emitting system (and are unaffected by the system’s distance and orientation with respect to the component detectors). Note that $\eta(t)$ is the envelope of the more rapid $\sin \zeta(t)$ and $\cos \zeta(t)$ oscillations; the structure of $\eta(t)$ and $\zeta(t)$ beyond this is not relevant to the rest of our analysis [2].

The response of any single detector in the network to this strain is

$$m(t) = \frac{\eta(t)}{r} [(1 + \cos^2 \iota) \cos \zeta(t) F_+ + 2 \cos \iota \sin \zeta(t) F_\times], \quad (16)$$

where the antenna patterns F_+ , F_\times and source inclination ι encode the relative orientations of the emitting system and detector.

B. Analysis strategies

The output $g(t)$ of the detector also consists of noise $n(t)$, assumed to be additive with the signal response and sta-

tionary on the time scale of the signal,

$$g(t) = m(t) + n(t). \quad (17)$$

The noise component of the detector output can be made Gaussian by the application of a linear whitening filter ($'$), also stationary on the time scale of the signal,

$$g'(t) = m'(t) + n'(t). \quad (18)$$

The application of the filter also alters the response.

Following Finn [4], to determine with confidence if a particular signal response $m'(t)$ is present in the filtered output $g'(t)$ of a single detector, consider the mutually exclusive hypotheses H_0 , that the detector output consists solely of Gaussian noise $g'(t) = n'(t)$, and H_m , that the detector output consists of the sum of Gaussian noise and the filtered signal response, $g'(t) = n'(t) + m'(t)$. The *likelihood ratio* Λ is then the ratio of the probabilities of the observed output $g'(t)$ arising under each hypothesis,

$$\Lambda(g'|m') = \frac{P(g'|H_m)}{P(g'|H_0)} \quad (19)$$

$$= \frac{P(g' - m'|H_0)}{P(g'|H_0)}. \quad (20)$$

The likelihood may be readily computed by *matched filtering* [4],

$$\ln \Lambda(g'|m') = 2\langle g', m' \rangle - \langle m', m' \rangle, \quad (21)$$

where $\langle \cdot \rangle$ denotes the inner product of the two time series. This allows us to determine the ‘‘plausibility’’ that the detector output arose from any particular signal response.

The *maximum likelihood*

$$\Lambda_{\max}(g'|\mathcal{M}) = \max_{m \in \mathcal{M}} \Lambda(g'|m') \quad (22)$$

is the likelihood of the most plausible signal response \hat{m} in some set of responses \mathcal{M} . A *confident detection* of a candidate signal $\hat{m} \in \mathcal{M}$ is said to have occurred when

$$\Lambda_{\max}(g'|\mathcal{M}) = \Lambda(g'|\hat{m}') > \Lambda_0, \quad (23)$$

where Λ_0 is a *threshold* value that is set sufficiently high to ensure that when no signal is present it is exceeded only at an acceptable *false alarm* rate. A *false dismissal* occurs when the likelihood for a weak but real signal fails to exceed the threshold.

A simple *coincident* network analysis can be performed using only the above algorithm on each detector: a detection occurs only when each observatory detects the signal \hat{m}_j . This requirement allows each threshold Λ_j to be lower than for the particular detector operating in isolation, as more frequent false alarms are ‘‘vetoed’’ by other detectors. For a network of identical detectors, the thresholds themselves are identical, so that a detection occurs when

$$\min_j \Lambda_{\max}(g'_j|\mathcal{M}) > \Lambda_{\text{coincident}}. \quad (24)$$

Alternatively, *coherent* network analysis vectorizes the maximum likelihood test to treat the network as a whole, a confident detection occurring when

$$\Lambda_{\max}(\mathbf{g}'|\mathcal{M}) > \Lambda_{\text{coherent}}, \quad (25)$$

where $\mathbf{g}' = [g'_1 \dots g'_n]$. No single detector is required to meet any threshold. This technique is theoretically optimal in the same sense as the maximum likelihood test is optimal for a single detector. When the noise is uncorrelated between detectors in the network, the likelihood is separable, so that

$$\Lambda(\mathbf{g}'|\mathbf{m}') = \prod_{j=1}^n \Lambda(g'_j|m'_j), \quad (26)$$

but as the maximization occurs for the system as a whole,

$$\max_{m_j \in \mathcal{M}} \prod_{j=1}^n \Lambda(g'_j|m'_j) > \Lambda_{\text{coherent}}, \quad (27)$$

the individual signal responses m_j typically do not correspond to maximum likelihoods for the individual detectors [4].

C. Detection rate

We are concerned only with the case where a physical signal is present, as false alarms have been limited to an acceptably low rate.

Consider the gravitational wave signal from a particular binary inspiral event, with all parameters fixed except its distance to the detectors (corresponding to the inverse amplitude of the wave: Eq. (13)). We may establish an effective maximum distance $r_{\max}(\theta, \phi)$ beyond which the probability of detecting such a source falls below some threshold. This value could be computed from the definitions of the tests above, for example, by Monte Carlo simulation.

Consider a population of otherwise identical binary inspiral systems uniformly distributed in (flat) space and randomly oriented. The effective volume V of space in which the events can be detected can be computed from r_{\max}^3 by integrating over the sky and averaging over source orientation and inclination,

$$V = \frac{1}{12\pi} \int_0^\pi d\iota \sin(\iota) \times \int_0^{2\pi} d\psi \int_{-\pi}^\pi d\phi \int_{-\pi/2}^{\pi/2} d\theta \cos\theta r_{\max}^3. \quad (28)$$

For a constant event rate per unit volume ρ , the rate of confident detections from the network is ρV .

This constitutes a valid figure of merit $f = \rho V$. A network with a higher rate of detections (for the same level of confidence) is clearly better than a network with a lower rate of detections, at least so far as detection of this particular class of binary inspirals is concerned.

This figure of merit is, however, prohibitively expensive to compute naïvely. Instead, we simplify it and introduce approximations to implement a new, computable figure of merit.

D. Implementation

From Eq. (16),

$$m'(t) = [\eta(t) \cos \zeta(t)]' \frac{1 + \cos^2 \iota}{r} F_+ + [\eta(t) \sin \zeta(t)]' \frac{2 \cos \iota}{r} F_\times. \quad (29)$$

Noting that

$$\langle (\eta \cos \zeta)', (\eta \cos \zeta)' \rangle \approx \langle (\eta \sin \zeta)', (\eta \sin \zeta)' \rangle, \quad (30)$$

$$\langle (\eta \cos \zeta)', (\eta \sin \zeta)' \rangle \approx 0, \quad (31)$$

then when a signal m' is present

$$\begin{aligned} \ln \Lambda(g'|m') &= 2\langle m' + n', m' \rangle - \langle m', m' \rangle \\ &= \langle m', m' \rangle + 2\langle n', m' \rangle \end{aligned} \quad (32)$$

$$\begin{aligned} &\approx \langle (\eta \cos \zeta)', (\eta \cos \zeta)' \rangle \frac{1}{r^2} [(1 + \cos^2 \iota)^2 F_+^2 \\ &\quad + 4\cos^2 \iota F_\times^2] + 2\langle n', m' \rangle. \end{aligned} \quad (33)$$

We assume that for confident detections

$$\ln \Lambda_{\max}(g') \approx \ln \Lambda(g'|m') \approx \overline{\ln \Lambda(g'|m')}, \quad (34)$$

where $\langle \rangle$ is expectation value; in other words, that the most plausible signal approximates the real signal, and that the contribution of noise to the likelihood is negligible.

Under this assumption, the coincident test in Eq. (24) becomes

$$\begin{aligned} \ln \Lambda_{\text{coincident}} &< \overline{\ln \Lambda(g'_j|m'_j)} \\ &= \frac{\langle (\eta \cos \zeta)', (\eta \cos \zeta)' \rangle}{r^2} \min_j [(1 + \cos^2 \iota)^2 (F_+)_j^2 \\ &\quad + 4\cos^2 \iota (F_\times)_j^2], \end{aligned} \quad (35)$$

and the coherent test in Eq. (27) becomes

$$\begin{aligned} \ln \Lambda_{\text{coherent}} &< \ln \prod_j \overline{\Lambda(g'_j|m'_j)} \\ &= \frac{\langle (\eta \cos \zeta)', (\eta \cos \zeta)' \rangle}{r^2} \sum_j [(1 + \cos^2 \iota)^2 (F_+)_j^2 \\ &\quad + 4\cos^2 \iota (F_\times)_j^2]. \end{aligned} \quad (36)$$

The two tests differ only in their use of min or \sum to combine the likelihoods.

The maximum detectable distance r_{\max} is the distance at which the threshold is reached; for a coincident analysis

$$r_{\max}^2 = \frac{\langle (\eta \cos \zeta)', (\eta \cos \zeta)' \rangle}{\ln \Lambda_{\text{coincident}}} \min_j [(1 + \cos^2 \iota)^2 (F_+)_j^2 + 4\cos^2 \iota (F_\times)_j^2], \quad (37)$$

and for a coherent analysis

$$r_{\max}^2 = \frac{\langle (\eta \cos \zeta)', (\eta \cos \zeta)' \rangle}{\ln \Lambda_{\text{coherent}}} \sum_j [(1 + \cos^2 \iota)^2 (F_+)_j^2 + 4\cos^2 \iota (F_\times)_j^2]. \quad (38)$$

Then,

$$\begin{aligned} V_{\text{coincident}} &\propto f_{n,\Theta,\text{coincident}} \\ &\propto \int_{\Omega} \left\{ \min_j [(1 + \cos^2 \iota)^2 (F_+)_j^2 + 4\cos^2 \iota (F_\times)_j^2] \right\}^{3/2} \cos \theta \sin \iota d\Omega, \end{aligned} \quad (39)$$

$$\begin{aligned} V_{\text{coherent}} &\propto f_{n,\Theta,\text{coherent}} \\ &\propto \int_{\Omega} \left\{ \sum_j [(1 + \cos^2 \iota)^2 (F_+)_j^2 + 4\cos^2 \iota (F_\times)_j^2] \right\}^{3/2} \\ &\quad \times \cos \theta \sin \iota d\Omega, \end{aligned} \quad (40)$$

where the neglected term $\langle (\eta \cos \zeta)', (\eta \cos \zeta)' \rangle$ depends only on the source class, and the thresholds $\Lambda_{\text{coincident}}$ and $\Lambda_{\text{coherent}}$ are assumed to depend only on the detector design. (We neglect the dependence of the thresholds on the geographical configuration of the network [15].)

The figures of merit $f_{n,\Theta,\text{coincident}}$ and $f_{n,\Theta,\text{coherent}}$ are (granted approximations) linearly proportional to the actual detection rate ρV . To evaluate these figures of merit, the response matrices \mathbf{R}_j are first computed for each detector using Eq. (5). Numerical Monte Carlo integration is implemented, randomly selecting source parameters from the population and evaluating the interior of the integral many times (using Eqs. (8) and (9) to compute the antenna patterns), and averaging the result.

E. Results

We may use our figures of merit, Eqs. (39) and (40), to answer a variety of questions about the network; we choose to determine the optimal detector location to augment an existing network of identical detectors.

Formally, consider a network of n detectors. Detectors 1 to $n - 1$ represent the existing detectors with fixed latitude θ_j , longitude ϕ_j and orientation ψ_j . Detector n represents the augmenting detector with variable latitude θ_n , longitude ϕ_n and orientation ψ_n . Effectively, we wish to compute the figure of merit f over the subset $\mathcal{T} \subset \mathcal{S}_{n,\Theta,\Xi} \subset \mathcal{N}$, where \mathcal{T} represents the 3-dimensional surface of constant θ_j, ϕ_j, ψ_j for $j < n$.

We can further reduce \mathcal{T} by noting that $f_{\text{coincident}}$ and f_{coherent} vary only weakly with ψ_n (see the end of this section). We may then additionally fix the orientation ψ_n

at an arbitrary value (we use $\psi_n = 0$, so that the detector is aligned North-South East-West), and consider only the 2-dimensional slice produced by varying θ_n and ϕ_n . (The LIGO Hanford and Livingston observatories are aligned to have antenna patterns as similar as possible, but this is more to ensure sensitivity to the same polarization than to ensure maximum power overlap.)

This 2-dimensional set has a straightforward interpretation as the geographical map of the merit of any site on the surface of the Earth to augment an existing network of $n - 1$ identical detectors with another such detector.

Consider first a single interferometer, at the site [8] of the LIGO Livingston Observatory (LLO). For a coincident network analysis, the merit of an additional site to augment LLO is given in Fig. 2. It demonstrates, as expected, that sites near or near-antipodal to LLO are best to augment it. This is the rationale behind the siting of the LIGO detectors. The worst configurations produce a substantially reduced detection rate; approximately 40% that of the optimal configuration.

It is interesting to note that for this simple case the map bears some resemblance to the “peanut” antenna pattern of the fixed single detector, with two prominent maxima and four minima; the weak directionality of the varying detector, and the superiority of a coaligned network [6] are responsible for this effect. This resemblance breaks down for more complicated networks.

Considering the same configuration of a fixed LLO detector and a varying detector with a coherent network analysis in Fig. 3, the qualitative structure of the map is similar, but quantitatively it is quite different. For a coherent analysis, the worst configurations produce a detection rate that is still 90% of optimal; site merit does not vary substantially with location.

The intentional similarity of the LIGO Hanford and Livingston detector alignments produces almost identical maps (Figs. 4 and 5) when considering both LIGO instruments; optimal sensitivity is achieved by adding a third instrument either nearby or antipodal to the existing instru-

ments. Unfortunately, the locations of the existing VIRGO, TAMA, and the proposed LCGT all fall in suboptimal locations, producing a detection rate of half that of an optimal site for a coincident search. As may be seen in Fig. 1, the antenna patterns of the American, European and Japanese sites point in almost orthogonal directions, so that any source will be poorly aligned with at least one—which is problematic for a coincident analysis that requires all detectors see the signal. The coherent detection rate is much less strongly affected by location, and though Europe and Japan are still among the worst sites to aug-

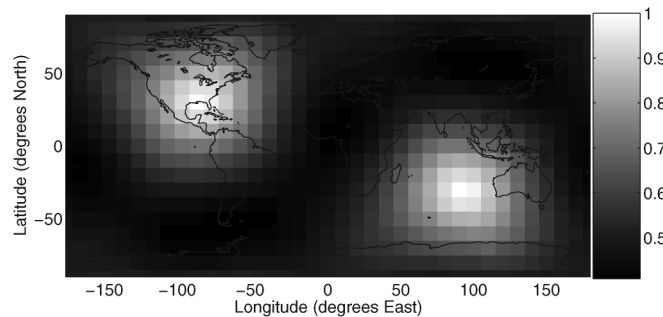


FIG. 2. Relative merit of an additional site to augment the LIGO Livingston Observatory in a coincident analysis, with coastlines overlaid for reference. Note that black is *not* zero sensitivity but rather the minimum sensitivity, in this case 41% of the maximum sensitivity.

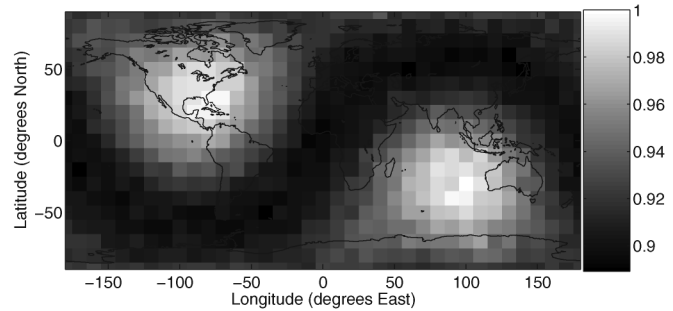


FIG. 3. Relative merit of an additional site to augment the LIGO Livingston Observatory in a coherent analysis.

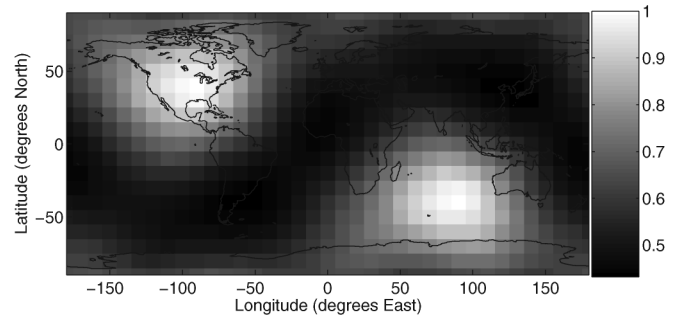


FIG. 4. Relative merit of an additional site to augment a network consisting of the LIGO Hanford (4 km) Observatory and the LIGO Livingston Observatory, in a coincident analysis.

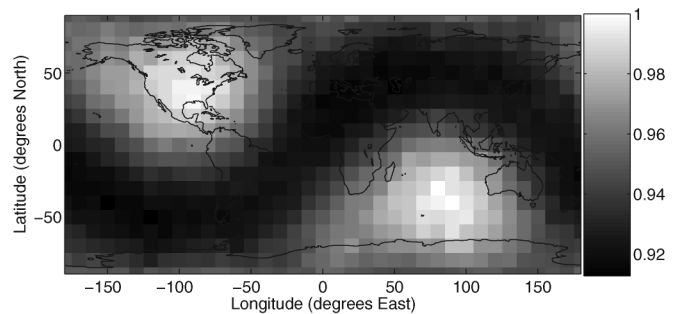


FIG. 5. Relative merit of an additional site to augment a network consisting of the LIGO Hanford (4 km) Observatory and the LIGO Livingston Observatory, in a coherent analysis.

ment LIGO, they are only 10% less sensitive than the best sites.

Note that in this, and all subsequent cases considered, among the best locations for both search strategies are North America and the coast of Western Australia. This is the rationale for the Gin-gin site of the proposed Australian International Gravitational Observatory. The advantage is typically pronounced for coincident analyses, but slight (or insignificant) for coherent analyses.

We now move on to consider an approximation to the existing global network of the larger interferometric gravitational wave detectors. We model the LIGO-VIRGO network as three identical interferometers at the sites of LIGO Hanford Observatory (LHO), LIGO Livingston Observatory and VIRGO [8]. Note that this model neglects the 2 kilometer LHO instrument, and the differences between the LIGO and VIRGO instruments. Similarly, we augment this three-detector network with a fourth (identical) detector at different locations and compare the relative detection rates of the resulting networks.

Using a coincident network analysis in Fig. 8, we see that the merit of the network varies moderately with location, with multiple minima of about 70% of the best achievable detection rates. Under a coherent network analysis in Fig. 9, we once again see a qualitative similarity to Fig. 8 in the locations of maxima and minima, but quantitatively much less variation than in the coincident case, with only 6% separating the best and worst sites.

A (less realistic) network of three detectors is to consider the LIGO sites and an instrument of comparable sensitivity at the TAMA site; this is perhaps a reasonable model for an Advanced LIGO and LCGT network, such as might occur during the downtime of VIRGO or a future European contributor. The quantitative results in Figs. 6 and 7 are comparable to the LIGO-VIRGO network though the larger separation of the LIGO and TAMA sites changes the qualitative form of the map somewhat.

A network of four comparable detectors with two in North America, one in Europe and one in Japan, such as we might see when the LCGT comes online, is presented in

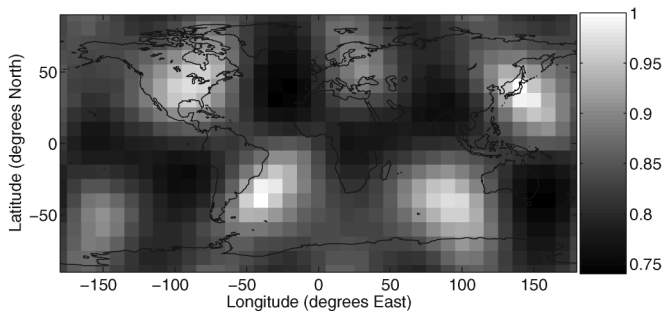


FIG. 6. Relative merit of an additional site to augment a network consisting of comparable instruments at the LIGO Hanford, LIGO Livingston and TAMA sites, in a coincident analysis.

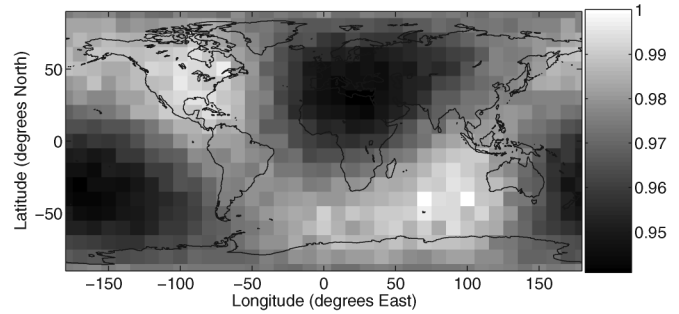


FIG. 7. Relative merit of an additional site to augment a network consisting of comparable instruments at the LIGO Hanford, LIGO Livingston, and TAMA sites, in a coherent analysis.

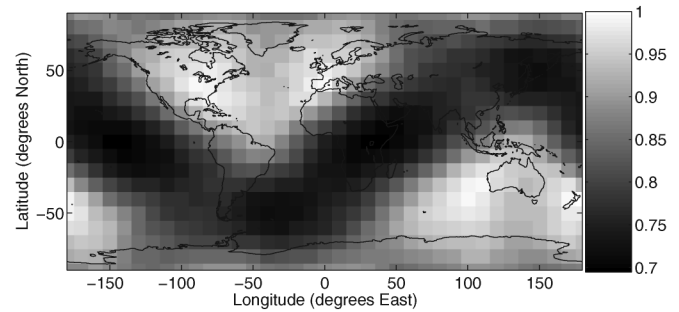


FIG. 8. Relative merit of an additional site to augment a network consisting of comparable instruments at the LIGO Hanford, LIGO Livingston, and VIRGO sites, in a coincident analysis.

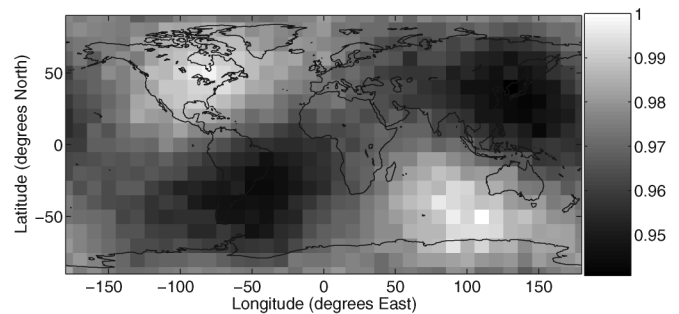


FIG. 9. Relative merit of an additional site to augment a network consisting of comparable instruments at the LIGO Hanford, LIGO Livingston, and VIRGO sites, in a coherent analysis.

Figs. 10 and 11. With so many detectors covering the sky, the position of a fifth detector has almost no impact on the coherent detection rate of the five-detector network. The impact on the coincident analysis, however, is still pronounced, with bad sites producing 25% fewer detections than the best.

Varying the n -th detector orientation ψ_n at a fixed location produces changes of approximately 9% and 2%, respectively, in the coincident and coherent 2-detector

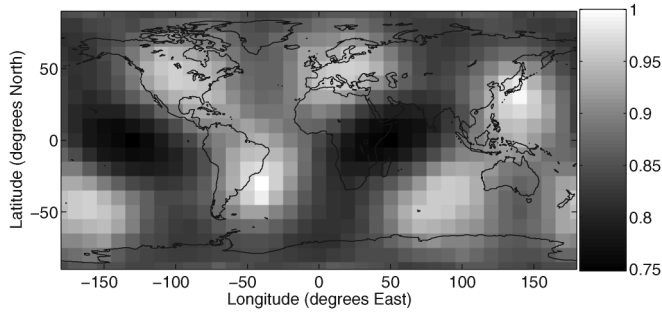


FIG. 10. Relative merit of an additional site to augment a network consisting of comparable instruments at the LIGO Hanford, LIGO Livingston, VIRGO, and TAMA sites, in a coincident analysis.

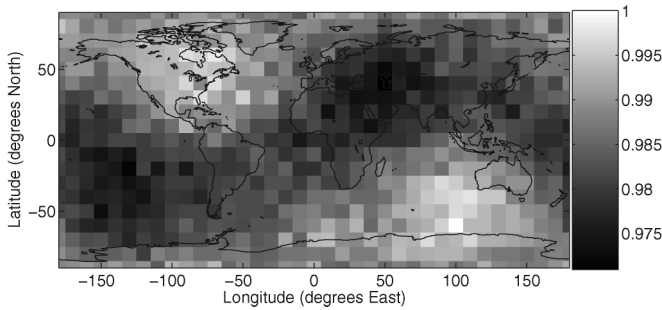


FIG. 11. Relative merit of an additional site to augment a network consisting of comparable instruments at the LIGO Hanford, LIGO Livingston, VIRGO, and TAMA sites, in a coherent analysis.

networks with Livingston fixed (Figs. 2 and 3), smaller than the effect of location. The effect becomes even smaller as more detectors are added to the network and is always dominated by location.

IV. DETECTION OF CONTINUOUS GALACTIC SOURCES

The most optimistic estimates place the strain produced by continuous wave sources at least 3 orders of magnitude below those of inspiral and other burst events [16]. Hopes of their detection are due to the fact that the signal can be integrated over months, or potentially even years of observation.

The motions of the Earth serve to modulate the incoming continuous gravitational wave signal. Daily rotation varies the angle of the source, and hence the sensitivity of the detector, leading to variations in amplitude. Orbital motions provide a seasonally-varying Doppler shift to the frequency.

Currently, it is computationally unfeasible to cover all the possible parameters governing the waveform (as is done with template banks for inspirals). Optimal searches are restricted to match the parameters of pulsars known from their electromagnetic emissions [16]. Hierarchical

searches are computationally possible (though expensive and with less-than-optimal sensitivity), and are used to search for continuous wave sources not associated with electromagnetically identified pulsars. Einstein@Home is a current massively parallel hierarchical search using donated idle time on tens of thousands of CPUs [17].

A. Waveform, response, and population

Consider a neutron star and an interferometric gravitational wave detector. The neutron star has principal axes I_1 , I_2 and I_3 , and rotates about I_3 with angular frequency ω_p . The neutron star is a distance r from the detector, and I_3 is inclined at an angle i to the line of sight and is oriented at an angle ψ_p from geographic North. The strains produced for the two polarizations along the line of sight are

$$h_+(t) = \frac{\omega_g^2 I \varepsilon}{r} \left(\frac{1 + \cos^2 i}{2} \right) \cos \omega_g t, \quad (41)$$

$$h_\times(t) = \frac{\omega_g^2 I \varepsilon}{r} \cos i \sin \omega_g t, \quad (42)$$

where

$$I = \frac{I_1 + I_2}{2} \quad (43)$$

$$\varepsilon = \frac{I_1 - I_2}{I} \quad (44)$$

$$\omega_g = 2\omega_p, \quad (45)$$

noting that the frequency of the gravitational waves ω_g is twice that of the pulsar. A nonzero ε will be produced by a “mountain” or other asymmetry of the neutron star. The strain measured by the observatory will be

$$h(t) = F_+ h_+(t) + F_\times h_\times(t), \quad (46)$$

where the antenna-pattern factors F_+ and F_\times are functions of the (time-varying) relative orientation of the neutron star and the detector.

$$h(t) = \frac{\omega_g^2 I \varepsilon}{r} \left[F_+ \left(\frac{1 + \cos^2 i}{2} \right) \cos \omega_g t + F_\times \cos i \sin \omega_g t \right] \quad (47)$$

This is a sinusoid of some amplitude A and phase β

$$h(t) = A \cos(\omega_g t + \beta), \quad (48)$$

where

$$A^2 = \left(\frac{\omega_g^2 I \varepsilon}{r} \right)^2 \left[F_+^2 \frac{(1 + \cos^2 i)^2}{4} + F_\times^2 \cos^2 i \right]. \quad (49)$$

We neglect motions of the Earth (and indeed the neutron star) other than their rotation.

As the Earth, and any ground-based interferometer, rotates once each sidereal day, the value of A^2 will vary

with this period, T . The average over one sidereal day is equal to the average over right ascension,

$$\overline{A^2} = \left(\frac{\omega_g^2 I \varepsilon}{r}\right)^2 \frac{1}{2\pi} \int_{-\pi}^{\pi} F_+^2 \frac{(1 + \cos^2 i)^2}{4} + F_\times^2 \cos^2 i d\phi_p, \quad (50)$$

where the parameters of the observatory (most importantly, its latitude and orientation) are implicit in the antenna patterns.

A simple model of neutron star distribution in the galaxy is provided by [18]. For a population of neutron stars with a particular set of intrinsic parameters, we can determine what proportion of the total galactic population may be detected by a particular observatory for a particular threshold.

The result for any given threshold may be computed as a Monte Carlo integration, but the same computation can be used to simultaneously compute the fraction for any threshold. We store all the thresholds computed in the Monte Carlo sum, and sort it into a monotonically-decreasing list $(\overline{A^2})_i$. For a particular threshold $(\overline{A^2})_i$, its normalized position in the list i/N is the detectable population fraction.

B. Results

Figure 12 shows this relation for a variety of detector latitudes and orientations. As we would expect, in the regimes of very high and very low sensitivity, the position of the detectors is irrelevant. Even at intermediate sensitivities, however, the siting of an observatory has only a minimal impact. Strain sensitivity, not geometry, domi-

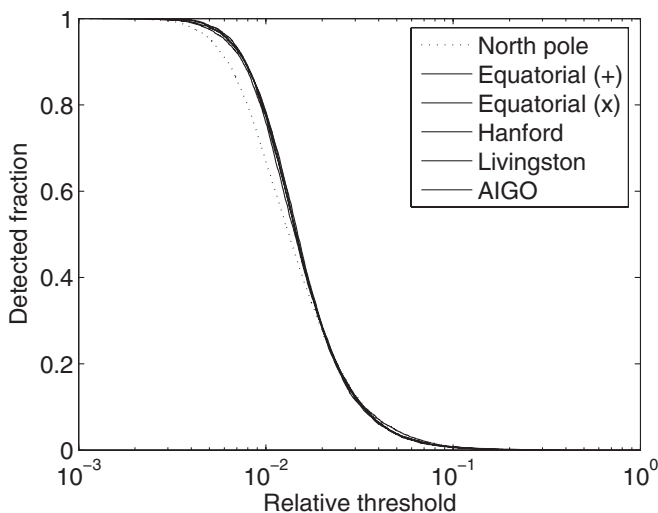


FIG. 12. Detectable fraction (vertical) of a galactic pulsar population against relative detection threshold (horizontal) for various detector latitudes and orientations (lines). The latitude and orientation have a minimal effect on a detector's ability to observe galactic neutron stars, which is almost wholly governed by its baseline strain sensitivity.

ates. Despite the large differences in the sidereally-averaged antenna patterns of terrestrial gravitational wave observatories at different latitudes, the fraction of a galactic population of neutron stars they can detect is almost independent of latitude. (Of course, their ability to detect any particular neutron star is highly dependent on latitude.)

V. DISCUSSION

We have proposed a formalism for conducting studies of the relative merits of differently configured systems of gravitational wave observatories and different collaborative analysis techniques.

Under our model, it is clear that the binary inspiral detection rate for a global network is insensitive to the geographical configuration of its component detectors when a coherent analysis is used, in contrast to when a simple coincident analysis is used. Whilst the LIGO detectors and the proposed AIGO detector are well sited to complement one another under a coincident analysis, the sites of the VIRGO detector and the proposed LCGT detector are far from optimal; our results demonstrate that under a coherent analysis the cost of this suboptimal siting is substantially reduced, on at least one figure of merit. In this sense, the real global network is closer to optimal for a coherent analysis than for a coincident analysis. Our results also indicate that since, under a coherent analysis, detection rate is insensitive to detector siting, the location of an augmenting detector could be optimized for other network properties (for example, directional resolution) without compromising the event rate.

It is important to note that the model does not compare the absolute detection rates for the two analysis techniques; we cannot say that one method would produce a higher detection rate than the other for a given false alarm rate.

Another application of our formalism, to investigate the effect of observatory latitude on the detectability of a galactic population of continuous wave sources, revealed that despite a nonuniform distribution of sources across the sky and the nonuniform directional sensitivity of the detectors, the effect on detection rate was still minimal.

VI. CONCLUSION

We considered the detection of known short waveforms—the classic inspiral source, though our model is more widely applicable—by two different analysis techniques: the simple coincident test, and a fully coherent search (analogous to aperture synthesis in radio astronomy). By varying the location of one interferometer while keeping the others—corresponding to existing observatories—fixed, and performing a Monte Carlo estimate of the sensitivity of the whole network, we were able to plot the relative merit of new observatory locations. Western Australia, by virtue of its antipodean location to the

USA, was always an optimal position. The difference between the best and worst configurations for a coherent search was only a few percent suggesting that a coherent search is more robust against misalignment and thus more likely to suit a real global network. Similarly, when considering the detection of continuous wave sources—specifically a galactic population of neutron stars—only a slight dependency on detector latitude was observed, eliminating this as an important factor in siting an additional detector.

The models used are plausible, but for computational tractability a large number of simplifications had to be made—most importantly the assumptions of identical interferometers and neglecting issues of frequency response and the impact of environmental noise.

As well as more detections, another benefit of additional detectors is to improve the angular resolution of the network as a whole. In this respect, the long baseline between a Western Australian site and all of the Northern Hemisphere detectors is another point in its favor.

ACKNOWLEDGMENTS

The authors wish to thank the Australian Research Council (ARC) and the Australian Partnership for Advanced Computing (APAC) for their support. L.S.F. was supported by NSF award PHY 00-99559 and the Center for Gravitational Wave Physics, which is funded by the NSF under cooperative agreement No. PHY 01-14375.

-
- [1] P. Jaranowski and A. Krolak, *Phys. Rev. D* **49**, 1723 (1994).
 - [2] L. S. Finn and D. F. Chernoff, *Phys. Rev. D* **47**, 2198 (1993).
 - [3] P. Jaranowski, K. D. Kokkotas, A. Krolak, and G. Tsegas, *Classical Quantum Gravity* **13**, 1279 (1996).
 - [4] L. S. Finn, *Phys. Rev. D* **63**, 102001 (2001).
 - [5] A. Pai, S. Dhurandhar, and S. Bose, *Phys. Rev. D* **64**, 042004 (2001).
 - [6] N. Arnaud, M. Barsuglia, M.-A. Bizouard, F. Cavalier, M. Davier, P. Hello, and T. Pradier, *Phys. Rev. D* **65**, 033010 (2002).
 - [7] A. C. Searle, S. M. Scott, and D. E. McClelland, *Classical Quantum Gravity* **19**, 1465 (2002).
 - [8] B. Allen, gr-qc/9607075.
 - [9] W. E. Althouse, S. D. Hand, L. K. Jones, A. Lazzarini, and R. Weiss, *Rev. Sci. Instrum.* **72**, 3086 (2001).
 - [10] W. G. Anderson, P. R. Brady, J. D. E. Creighton, and E. E. Flanagan, *Phys. Rev. D* **63** 042003 (2001).
 - [11] D. E. McClelland, S. M. Scott, M. B. Gray, D. A. Shaddock, B. J. Slagmolen, A. C. Searle, D. G. Blair, L. Ju, J. Winterflood, and F. Benabid *et al.*, *Classical Quantum Gravity* **18**, 4121 (2001).
 - [12] D. E. McClelland (private communication).
 - [13] A. Brillet (private communication).
 - [14] M. Ando (private communication).
 - [15] Thanks to Peter Shawhan for pointing this out.
 - [16] B. Abbott *et al.*, *Phys. Rev. D* **69** 082004 (2004).
 - [17] *Einstein@Home*, <http://einstein.phys.uwm.edu>.
 - [18] S. J. Curran and D. R. Lorimer, *Mon. Not. R. Astron. Soc.* **276** 0 (1995).